Energy Building Sustainability by Optimized Daylight Tubes

Berta García-Fernandez[1], Antonio Álvarez Fernandez-Balbuena[2], Mikel Jaureguizar[3], Miguel Angel Garcia[3] and Daniel Vazquez-Moliní[2]

[1] ETSI Montes, Forestal y del Medio Natural, Dpto. de Ingeniería y Gestión Forestal y Ambiental, Centro de I+D+i para la Conservación de la Biodiversidad y el Desarrollo Sostenible (CBDS) Universidad Politécnica de Madrid, Madrid (Spain)

[2] Facultad de Óptica y Optometría, Departamento de Óptica Universidad Complutense de Madrid, Madrid (Spain)

[3] Normagrup, Asturias (Spain)

Abstract

New interest in Innovative Daylight Systems has emerged strongly because energy consumption must be reduced, and human environment conditions improved. Light propagated through prismatic films, exhibits a characteristic behavior optimal for energy savings, sustainability and environmental conservation. These optical particularities and capabilities can be useful for multiple applications in areas such as architectural lighting, automotive lighting, and display technology. Therefore, it is essential to consider the optical properties of these singular light guiding systems to control light energy and thus, accurate simulations and modeling are necessary to improve the designs. In this study, the application of Fresnel's equations is compared with basic Snell's law showing the angular propagation differences and the influence of defects in peak's prism is quantified. In this framework, a prototype in real scale has been developed and tested.

Keywords: Energy saving, Innovative Daylighting Systems, Daylighting, Light guides, Sustainability

1. Introduction

Saving energy is key to fighting climate change and reducing the energy dependency. Energy efficiency improvements could reduce not only CO_2 emissions, but also the bill for energy imports (Energy saving: EU action). Demand for lighting is continued increasing driven by strong growth in many fields like buildings or display technologies. Within this context, improving energy saving is essential by means of efficient lighting systems, which implies a truly exhaustive study of the optimal optical components of lighting systems for proper use. The use of natural light in buildings is very valuable because energy consumption can be reduced and human environment conditions can be improved (Sharp, 2014). Innovative Daylighting Systems (IDS) have been developed over the last few decades to increase daylight levels within buildings where it is not possible with simple windows or domes (Littlefair, 1994; Mayhoub, 2014; Kim, 2010). They improve and control daylight, minimize glare and reduce energy consumption. Hollow Light Guides (HLG) are IDS that channels light into the core of the buildings through long distances (Garcia-Fernandez, 2023; Osama Omar, 2018; Nair, 2014), they can transmit high-diameter light beams in daylight and artificial lighting applications without relevant losses. Hollow Prismatic Light Guides (HPLG) are made from a plastic transparent prismatic film with a plane surface on the inner side and prisms with right angle on the outer side. Prismatic films are especially valuable for their performance in light guiding and is used for multiple applications in areas such as daylight in architecture, lighting, solar concentrator systems, automotive illumination and displays (Xie B, 2015; Wang, 2015). Light introduced into the light guide at the appropriate angle range will be retained inside the guide and guided long distances due to the phenomenon of Total Internal Reflection (TIR) (García-Fernández, B, 2015). The multiple reflections of light existing in these optical guiding elements and their interaction with surface defects cause uncontrolled light that leaves the ideal optical ray pattern and increases exponentially with the distance travelled. Simulate accurately prismatic lighting systems performance is a complex task due to the amount of computation necessary to represent data of light paths. Thus, as a rule, calculations are usually made by the simple method based on approximations of the law of Snell, this procedure don't consider partial reflections or transmissions defined by Fresnel equations (Dupertuis, 1994; De Greve, 2006; Born, 2013). Within this context, this study presents a detailed analysis applied Snell's Law and Fresnel equations for all incident angles and shows the influence of a curved apex of the prism which simulates defects in corners. The defects in corners have been meassured by Scanning Electron Microscopy (SEM) based image analysis. Firstly, a theoretical study of optical properties was made using the Snell's law and Fresnel's equations. Secondly the defects in corner as key element of

Selection and/or peer review under responsibility of Scientific Committee
10.18086/eurosun.2024.01.02 Available at http://proceedings.ises.org

efficiency in guiding were tested by a ray-tracing software TracePro. Finally, experimental measurements were made to compare the simulated result with measured data.

2. Theoretical context Snell's law versus Fresnel equations

Snell's law gives the relationship between the incidence angle and refraction θ (or reflection θ') for a ray impinging on an interface between two media with different refraction index n (Fig.1). The Snell's Law is expressed as:

$$n \sin \theta = n' \sin \theta', \quad \text{(eq. 1)}$$

The vector form of Snell's Law is used for calculating the direction of transmitting light in software simulations by a coordinate-free formalism based on vector algebra.

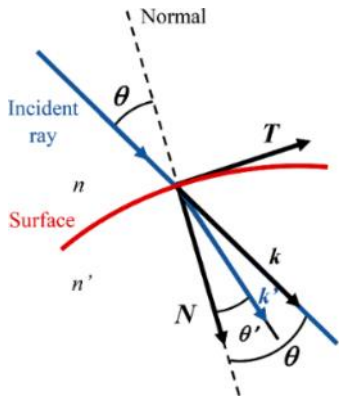

Figure. 1. Refractive optical surface represented by tracing vector rays

Writing Snell's law using the direction vectors of the incident and refracted rays' $\boldsymbol{k}$ and $\boldsymbol{k}'$ and the surface normal vector $\boldsymbol{N}$. These vectors are coplanar, so that both k and k 'may be expressed as a linear combination of two vectors in the plane of incidence, the normal $\boldsymbol{N}$ and the tangent vector $\boldsymbol{T}$. In figure 1, the incident ray is defined by a vector $\boldsymbol{k}$ with an angle of incidence θ. After refraction at the surface, the refracted ray is defined by a vector $\boldsymbol{k'}$ with an angle of refraction θ'. The normal to the surface at the point of intersection of the ray with the surface is denoted by a vector $\boldsymbol{N}$. We can define a vector in the plane of $\boldsymbol{k}$, $\boldsymbol{k'}$, and $\boldsymbol{N}$, and parallel to the surface at the point of incidence. This unit vector is denoted by $\boldsymbol{T}$. From Fig. 1 we can see that:

$$\boldsymbol{k} = \cos\theta\, \boldsymbol{N} + \sin\theta\, \boldsymbol{T}, \quad \text{(eq. 2)}$$

Hence, the vector in the direction of propagation is given by:

$$\boldsymbol{k}' = \cos\theta'\, \boldsymbol{N} + \sin\theta'\, \boldsymbol{T}, \quad \text{(eq. 3)}$$

Equation 2 can be combined with 3 to give

$$\boldsymbol{T} = \frac{\boldsymbol{k} - \boldsymbol{N}\cos\theta}{\sin\theta} = \frac{\boldsymbol{k'} - \boldsymbol{N}\cos\theta'}{\sin\theta'}, \quad \text{(eq. 4)}$$

Therefore,

$$(\boldsymbol{k} - \boldsymbol{N}\cos\theta)\sin\theta' = (\boldsymbol{k}' - \boldsymbol{N}\cos\theta)\sin\theta, \quad \text{(eq. 5)}$$

and, using Snell's law,

$$(\boldsymbol{k} - \boldsymbol{N}\cos\theta)n = (\boldsymbol{k}' - \boldsymbol{N}\cos\theta)n', \quad \text{(eq. 6)}$$

Finally, we can summarize with the general expression of Snell´s law written in vector form, which is given by the expression,

$$n'\boldsymbol{k}' - n\boldsymbol{k} = \boldsymbol{N}(n'\cos\theta' - n\cos\theta). \quad \text{(eq. 7)}$$

$$\boldsymbol{k}' = \frac{n\boldsymbol{k} + \boldsymbol{N}(n'\cos\theta' - n\cos\theta)}{n'}. \quad \text{(eq. 8)}$$

TIR occurs whenever the incident beam in the optically denser medium strikes the boundary at an angle of incidence equal to, or grater tan a critical angle given by:

$$\sin\theta_c = \frac{n_2}{n_1}. \quad \text{(eq. 9)}$$

The condition was defined purely geometrically by setting,

$$\theta' = \frac{\pi}{2} \quad \text{(eq. 10)}$$

Total Internal Reflection occurs whenever the incident beam in the optically denser medium strikes the boundary at an angle of incidence equal to, or grater tan a critical angle given by setting sin $\theta'=\theta$. In calculations, Fresnel reflection is based on refractive index and the complex index of refraction is defined by,

$$\check{n} = n + ik\,, \quad \text{(eq. 11)}$$

where k is the extinction coefficient defined as,

$$k = \frac{\lambda\alpha}{4\pi}. \quad \text{(eq. 12)}$$

λ is the wavelength and α is the absorption coefficient.

Fresnel equations describe the ratios of the reflected and transmitted waves' electric fields to the incident wave's electric field [14]:

$$t_s = \frac{2n\cos\theta}{n\cos\theta + n'\cos\theta'}, \quad \text{(eq. 13}$$

$$r_s = \frac{n\cos\theta - n'\cos\theta'}{n\cos\theta + n'\cos\theta'}, \quad \text{(eq. 14)}$$

$$r_p = \frac{n\cos\theta' - n_2\cos\theta}{n\cos\theta' + n_2\cos\theta}, \quad \text{(eq. 15)}$$

$$t_p = \frac{2n\cos\theta}{n\cos\theta' + n'\cos\theta}, \quad \text{(eq. 16)}$$

Power reflectivity and transmission is then calculated as,

$$R_{s,p} = \left|r_{s,p}\right|^2, \quad \text{(eq. 17}$$

$$T_{s,p} = \frac{n'\cos\theta'}{n\cos\theta}\left[t_{s,p}\right]^2. \quad \text{(eq. 18)}$$

The unpolarized case is computed as an average between *S* and *P* polarizations.

3. Application of Snell's law and Fresnel's equations for light propagation in prismatic dielectric films.

In this section, we report a computer simulation analysis of light transmission and reflexion in prisms comparing the results applying the Snell's law and the Fresnel's equations. Fresnel equations show a more detailed explanation of the process of light refraction and refraction at a boundary than Snell's law. The behavior of the right-angle prism as a function of the incident angles along the base of the prism has been studied by three-dimensional simulations performed in a non-sequential optical raytracing called TracePro [15]. The transparent optical material used is defined as continuous, homogeneous, perfect transmitter and non-absorbing. The incident light is assumed to consist of a plane wave of infinite extent. In simulations, the light rays enter through the base of a PMMA (Polymethylmethacrylate) prismatic structure and undergo TIR and refractions on the inner surfaces of the prism. Firstly, data processing was performed to evaluate light patterns. Secondly, a curved prismatic peak is developed and examined to assess the importance it can have in ray patterns and thus in transmission efficiency and guide of light.

The prismatic optical structure with an apex angle of a right-angle is characterized by polycarbonate material with a refractive index of 1.59 without consideration of absorption. Seven discrete equidistant quarter spheres (P1-P7) are inserted in the prismatic base to analyze the full angular range of light incidence and the flux ratio of light rays in several positions. The light source emits in the full angular range at a wavelength of 550 nm. The coordinate system

used defines the angles α and β are the direction cosines of the departing ray in X and Y axis. Rays emitted are propagated through the prism, undergoing refractions and reflections on the inner surfaces of the extruded prism. After analyzed ray behavior, the definite patterns of internal reflections and refractions within the material are computed. Figure 2 represents, at each position, the ray pattern obtained. The internal directionality happens through different patterns after the first refraction of a ray through the base of the prism. Firstly, a Double TIR of light (DTIR) occurs as is shown in Fig. 2 (a), in this case the light beam is guided along the interior material by means of two TIR following the Snell's law, and it returns to the base of the prism. In this pattern, some rays found are directed towards the left side (L) and other rays are directed towards the right side (R), depending on the internal surface on which ray effect. Secondly, a Multiple Internal Reflection (MTIR) occurs, in which one of the angles of the reflected ray is reversed (compare it with an ordinary specular reflection), in this case the beam undergoes three TIRs, as shown in Figure 2 (b). Finally, there are two patterns in which the rays are expelled to the outer upper surface. In one pattern, the beam is expelled after only one refraction through the prism side, Transmission 1 (TA1) shown in Figure 2(c). In the other pattern, the beam undergoes first a TIR and later, comes out by refraction through the prismatic side, Transmission 2 (TA2) (Fig. 2 (d)). From the point of view of the efficiency of a light pipe, TA1 and TA2 are considered the negative cases, since the necessary condition for guiding is not met. The prisms of Figure 2 represent the principal ray defined by Snell's law. There are reflected rays with lower energy which carry on the DTIR or MTIR pattern on the exit surface. This energy will be calculated by applying the Fresnel equations.

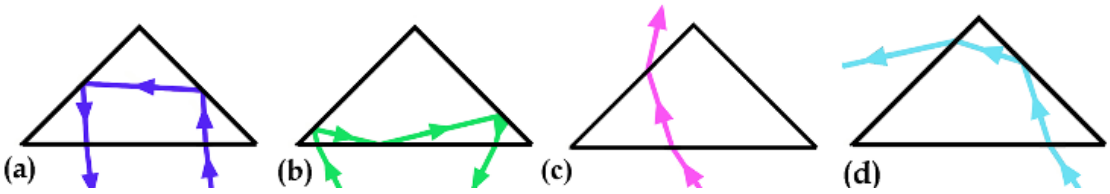

Figure. 2. Prism ray patterns evaluated; the arrows indicate the direction of the light beam. In the first figure (a), rays experience Double TIR (DTIR). In the second figure (b), the ray undergoes Multiple Internal Reflection (MTIR). Finally, in the last two patterns, the rays are expelled to the outside by Transmission (TA1) (c), and by TIR plus Transmission (TA2) (d)

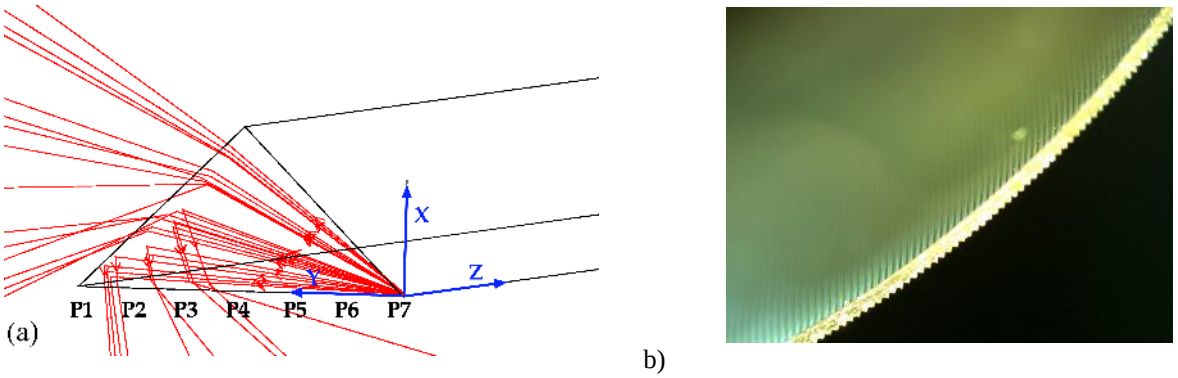

Figure. 7. Ray positions in Prismatic structure: P1, P2, P3, P4, P5, P6 and P7 (a). Perspective view of prismatic film (b). The ray flux is obtained for each pattern (Ro) defining the angular behaviors of each ray position (Fig. 7(a)). Figure 7 (b) shows a perspective view of the prismatic film.

2. 1. Snell's law versus Fresnel equations, ray path analysis in the prismatic structure

The optimization of light guidance is required in order to obtain more efficient lighting systems. Fresnel equations show a more detailed explanation of the process of light refraction and refraction at a boundary than Snell's law. Optical simulations were performed by the meaning of Snell' Law and Fresnel equations to make comparisons by processing the ray path information in MATLAB software.

Results of calculations are presented in Fig. 3, Fig. 5, Fig. 7. Figure 3 shows the angular range in degrees where TIR is produced by means of director angles (DTIR and MTIR), the positive directions of the coordinate axes are defined by alpha α, determined by the angle formed with the direction of the x axis, and beta β, defined as the angle formed with the positive direction of the y axis. By applying Snell's Law, the total flux of transmission (TA1 plus TA2) has constant values of 67.88%. Those who suffer TIR (MIR plus DTIR) are guided internally, add up to a value of 32.12 %. There is an angular range in which light acts by the phenomenon of TIR and will fulfill the condition to be transmitted internally in prismatic hollow guidance systems by numerous internal reflections. The boundary angle

condition (see Fig. 3 left) defines the angular range limit of TIR and within which rays are guided along the prism system.

Fresnel losses (Fig. 3 right) had been considered in simulations to improve accuracy. A new distribution appears, setting the angular range of rays that suffer internal reflections superimposing the previous ones. When comparing the coefficients of reflection and transmission obtained by applying the Fresnel Equations from an external incidence and comparing them with the transmittance and reflectance pattern calculated by applying Snell's Law, the amount of light transmitted outside (TA1 plus TA2) decreased from 67.88 % to ~51.56 %. Thus, results indicated a significant increase in light rays that suffer reflection plus TIR from 32.12 to ~ 48.32 %.

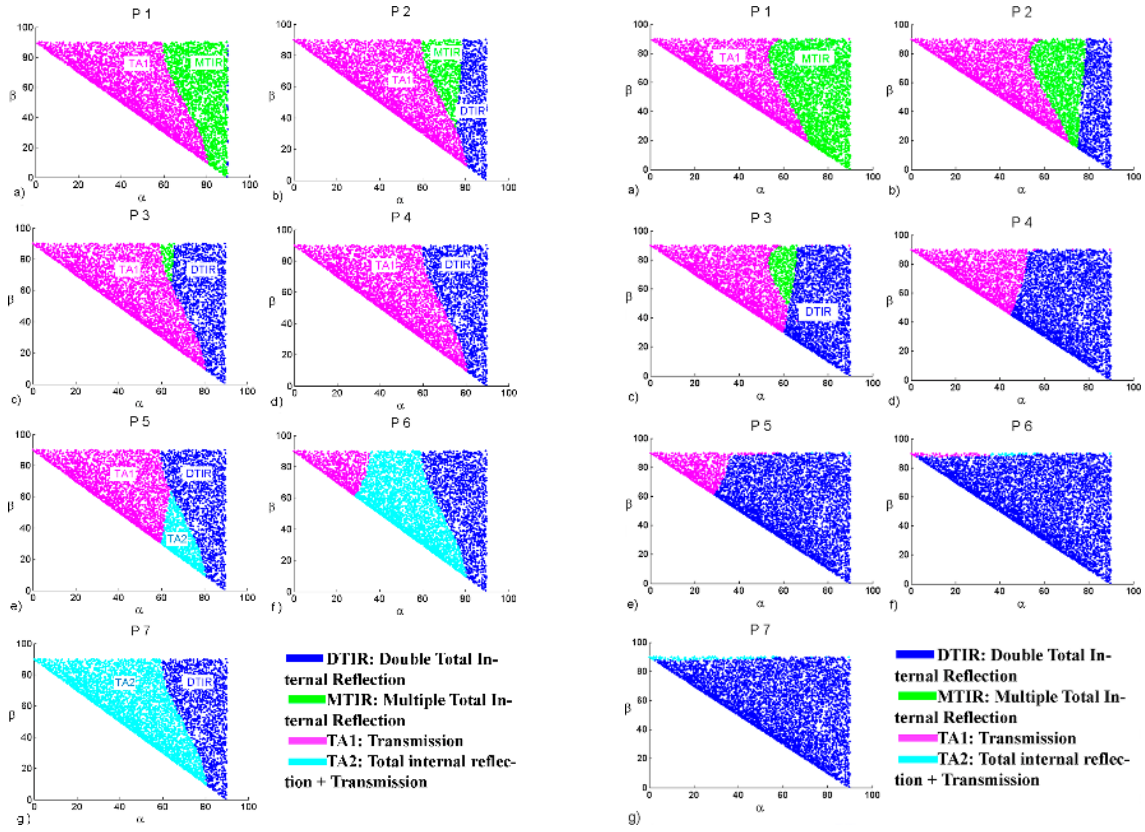

Figure. 3. (a) Graphs show the operation of light rays (P1-P7) in a perfect right angle prism by using a model based on the Snell's law (left) and Fresnel equations (right)

2.2. Scanning Electron Microscopic analysis, roughness influence

The defects were studied using Scanning Electron Microscopic (SEM-Tescan Mira 3). The image processing allows us to estimate a defect width of ~5-10 μm by measuring changes in surface roughness, which represents about 4.7% of prismatic surface. Defects in the surface have been identify in corners and defined by a curved region in simulations to compute the influence of corner defects in light guidance. Figure 4 shows the image of a prismatic peak obtained with Scanning Electronic Microscopy (SEM; Mira3 TESCAN).

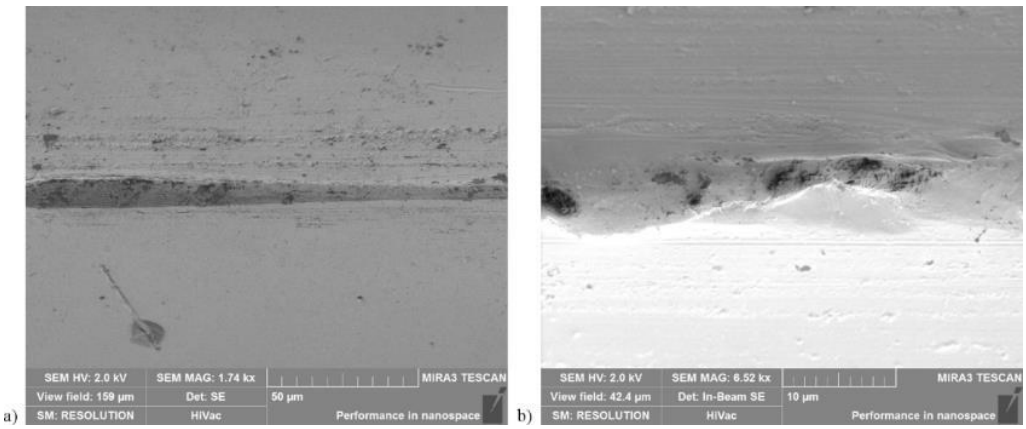

Figure. 4. Low (1.74 kX) (a) and high (6.52 kX) (b) magnification Scanning Electron Microscope (SEM) images of the

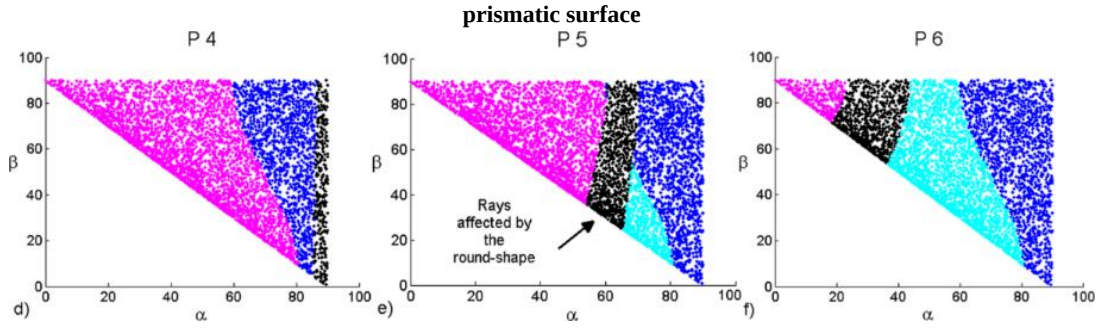

Figure. 5. Patterns of refracted and reflected rays located in positions P4, P5, P6 affected by rounded peaks (CP) in black color

Figure 5 shows in black color (CP) the rays affected by the round shape. The existence of the curved area on the peak of the prism modifies the optical path in positions P4, P5 and P6 and therefore the rays that impact over the rounded peak is redirected to other directions undergoing multiple internal reflections. In this case, many mixed patterns appear and some of those light rays are directed through the internal prism structure undergoing by multiple TIRs in the inner surfaces. Positions P1, P2, P3 and P4 are not affected by the rounded peak because no light strikes this surface. The influence of peak defects causes changes in behavior of rays. Thus, control the influence of defects on surfaces and objectify improvements in manufacturing processes are basic parameters in prismatic guidance systems.

2.3. Pattern classification ratio

Results are computed considering the angular distribution of a 90º quadrant (Fig. 8 (a)) and the total amount affected by a hemisphere emission range of 180 degrees (Fig. 8 (b) defined as.

$$R = \frac{R_o}{R_i} \quad , \qquad \text{(eq. 19)}$$

where Ri is the input flux and Ro represents the output flux.

The ratio associated with defined patterns for each position Figure 3 (left) and Figure 5 is given in Figure 8. The flux ratio obtained from patterns DTIR, TA1 and TA2, shows lower values than those found with perfect right angle peaks due to the rounded peak. The ratio of the rounded peak encompasses different light behaviors and rays that strike the inner surfaces of the prism and guide through the interior of the material.

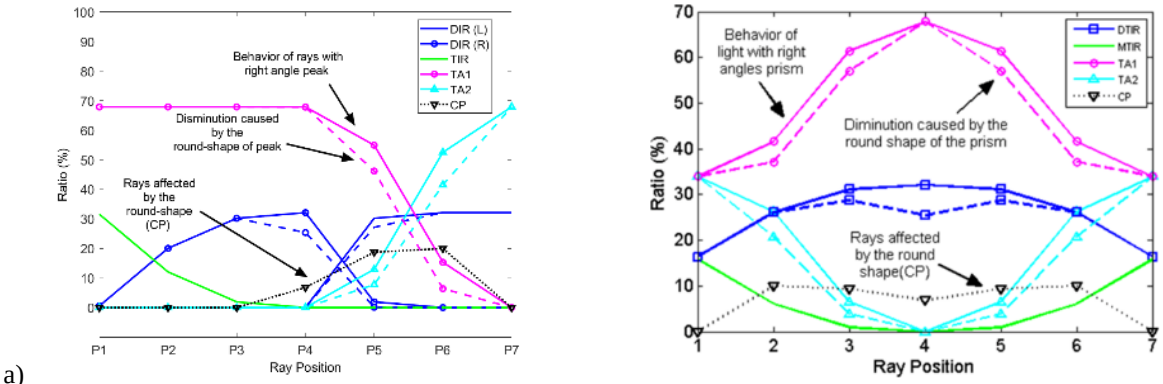

Figure 8. Patterns in a perfect prism for seven positions evaluated (continuous line). the angular behaviors of the rays considering an angular quadrant emission range (a) and the total amount affected by a hemisphere emission range of 180 degrees (b).

Tab. 1: Percentage of patterns affected by the perfect right angle prism and the curved right-angle prism

	Perfect Right Angle Prism	Curved Right Angle Prism
DTIR	25	24
MTIR	7	7
TA1	49	46
TA2	19	17

CP	-	7

4. Polar Intensity Distribution

The polar intensity distributions of the perfect right angle prism by applying Snell and Fresnel equations are shown in Figure 9 (a) and (b) and the light distribution produced in a rounded right angle prism simulating defects in apex is represented in Figure 10 (a) and (b). The Polar Luminous Intensity Graph illustrates the distribution of luminous intensity, in candelas, for the transverse (blue line) and axial (red line) planes of the luminaire. The curve in Figures 8 and 9 (a) shown the type of distribution expected from the prism acting as light source with side emitting pattern of peak intensity in 50º and semi-indirect. The curve in Figures 8 and 9 (b) shows the type of distribution expected from the prism with a rounded in peak.

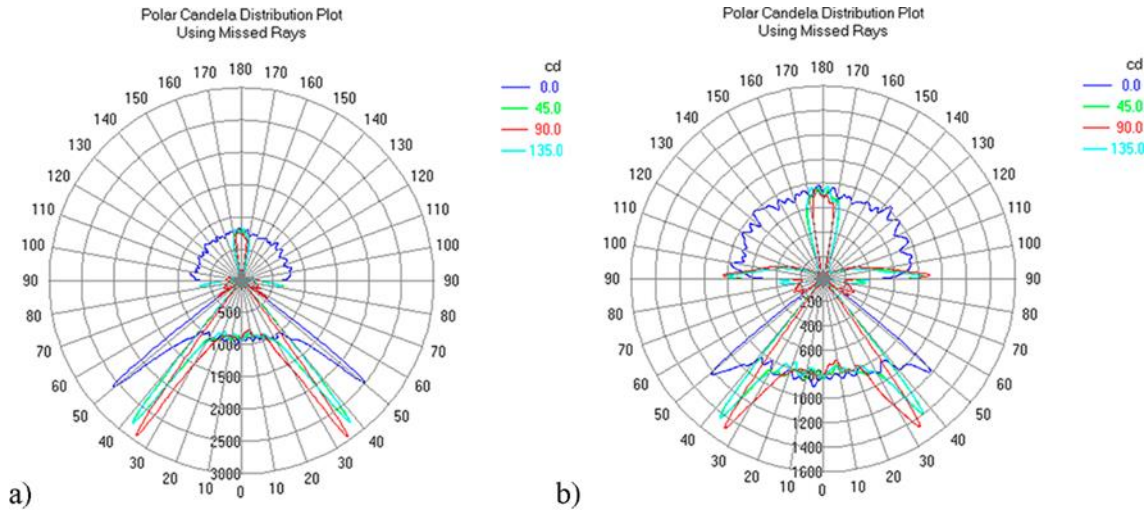

Figure. 9. Intensity distribution curves generated by applying Snell (a) and Fresnel (b) equations in a perfect right angle prism

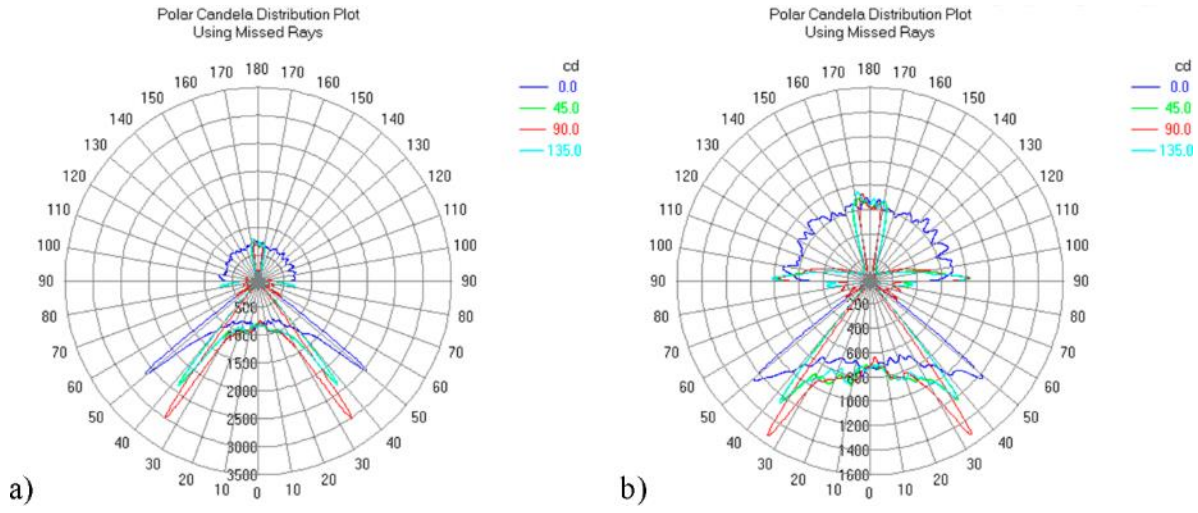

Figure 10. Intensity distribution curves generated by applying Snell (a) and Fresnel (b) equations with a rounded in peak

5. Hollow Light Guide Prototype: Laboratory Testing

This section shows an experimental model consisting of a 1:5 scale Hollow Prismatic Light Guide (HPLG), designed to illuminate a 47.52 m2 office space with natural light. The rectangular light guide has 2 m length, and the aperture side is 0,1 m, this HPLG simulates a big one of 10 m length and 0,5 m the aperture side, this corresponds to an aspect ratio of 20. Figure 11 shows a Schematic representation of the light pipe illumination device in section (a) front elevation (b) floor plant (c) and the first state of the prototype experimental mock-up (d).

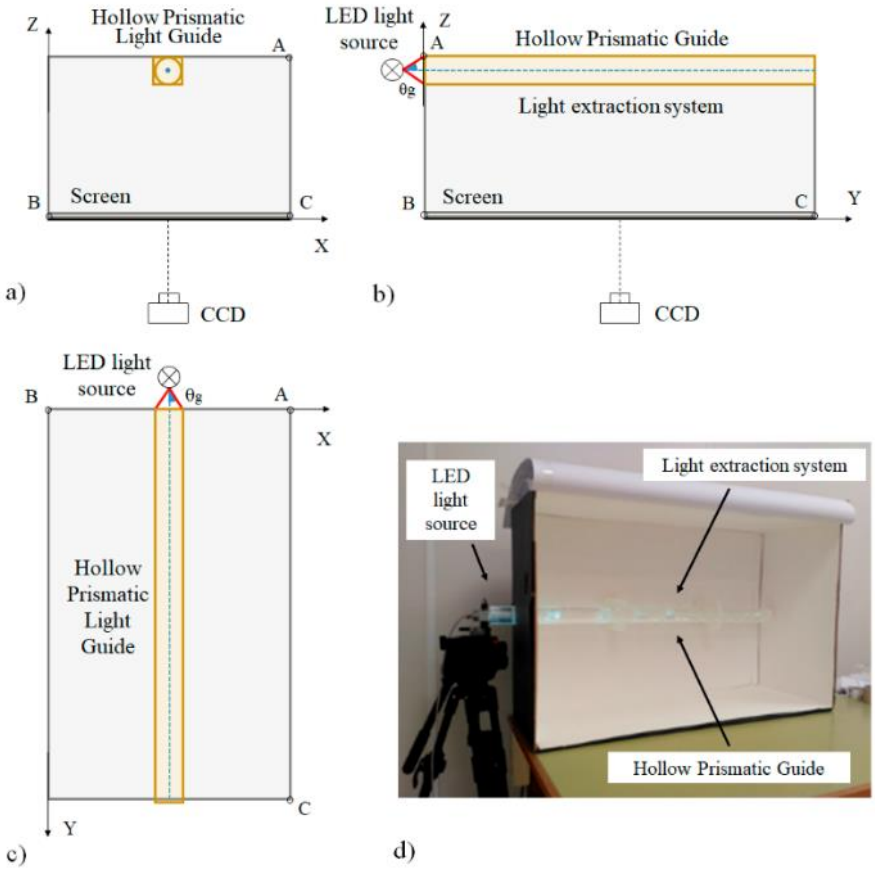

Figure 11. Schematic representation of the light pipe illumination device. (a) Section (b) Front elevation (c) Floor plant (d) Experimental mock-up. (b)

Figure 12 (a) shows the lateral view of the specified light pipe configuration. Figure 12 (a.1) illustrates the light distribution along the guide based on the characteristic exponential decay of the HPLG [11]. Figure 12 (a.2) represents the light behavior of a HPLG by optimizing light distribution along the guide with a light extraction system. Figure 12 (b) shows the cross-section of a Rectangular HPLG (b.1) and Cylindrical HPLG (b.2). The HPLG prototype with a rectangular light pipe (Fig. 12 (c)), a hemispherical screen collects the flux through a diaphragm appointed by a diaphragm designed to determine the light distribution. The luminous intensity distribution obtained is represented by Dialux software (Fig. 12 (d)). Figure 12 (e) shows the light distribution obtained in a square screen of the experimental mock-up. The light source is a LED which provides white uniform lambertian lighting within an angular acceptance of semiangle cone θg 30º according to the prismatic guide acceptance angle. Figure 12 (f) shows the illuminance map obtained in the experimental setup.

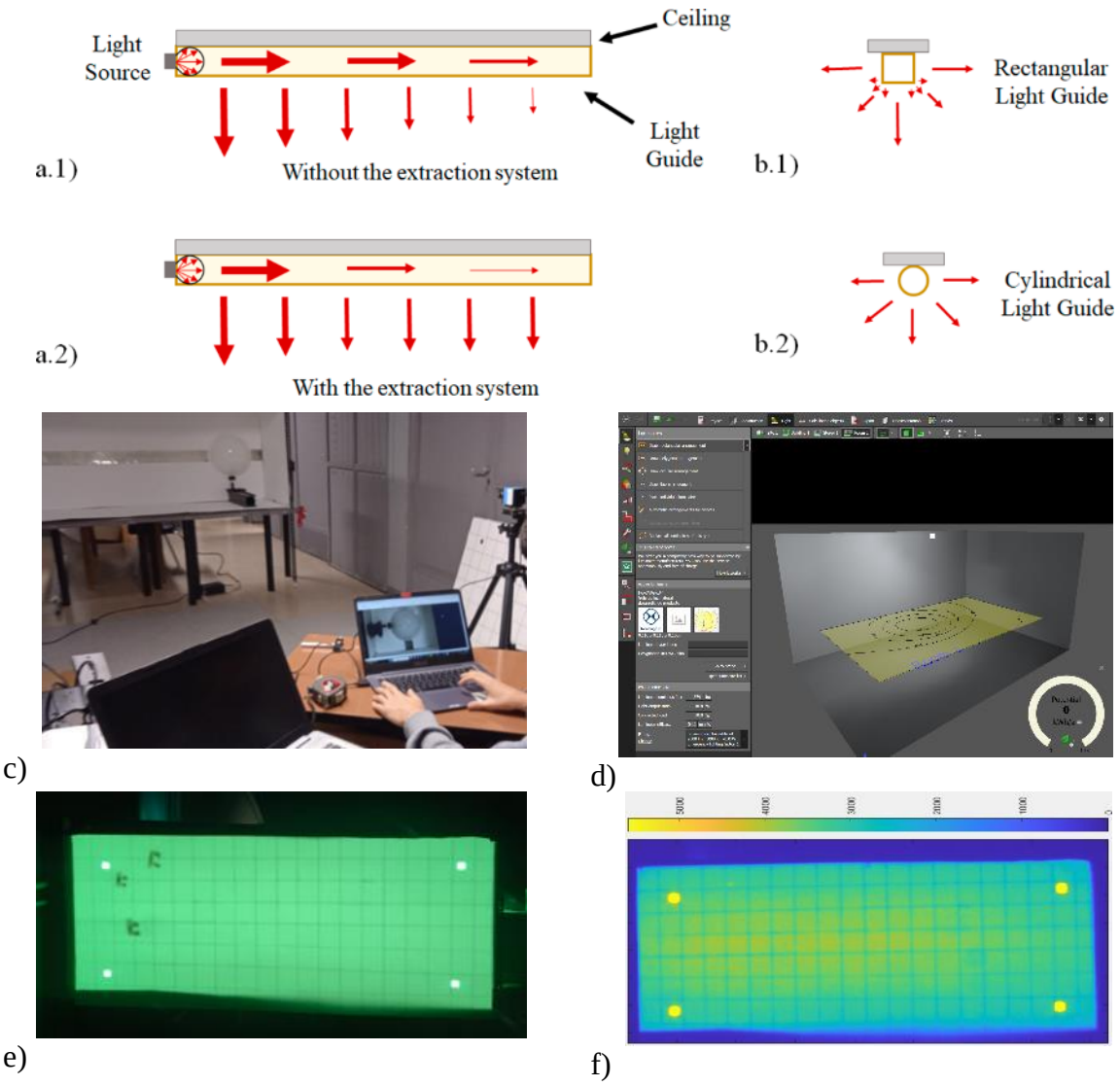

Figure 12. HPLG without extraction system (a.1) and with extraction system (a.2). The cross-section of a Rectangular HPLG (b.1) and Cylindrical HPLG (b.2). The experimental mock-up of a rectangular HPLG for photopic characterizing (c). Luminous Intensity distribution by Dialux software (d). Experimental setup image, illuminance measurement plan (e). Illuminance map of experimental setup.

6. Conclusions

Prismatic films are optical elements widely used due to its many practical applications as panel displays, renewable and green energy solutions and lighting. In this paper is presented the photometric characterization of prismatic film used in Hollow Prismatic Light Guides used to improve lighting, control daylight, minimize glare and reduce energy consumption through a new way to establish boundary conditions. The present study shows a novel classification of light transmission and the reflection properties in right angle dielectric prism by comparison of the flux rate calculated using Snell's law and Fresnel equations as a function of incidence angle and position in the prism base. Results based on Fresnel equations show a significant increase in light rays that suffer reflection plus TIR, so the total flux ratio goes from 32.12 % (Snell) to ~48.32 % (Fresnel). Scanning electron microscopy analysis shows the defects in prism's surfaces mainly located in peaks. Analysis shows that peak irregularities cause changes in behavior of rays of the order of 7% in the case of 4.7% width, this percentage is exponentially increasing due to multiple reflections in light guiding. Hence, control the influence of defects on surfaces and objectify improvements in manufacturing processes would be very advantageous for prismatic guidance performance. In this framework, a light guide in real scale has been developed and tested obtaining a uniform light distribution in the measurement plane according to the photometry of the prismatic guide.

7. Acknowledgments

This work has been funded by Normagrup and the Economic Development Institute of the Principality of Asturias: PID-1-II-23-006

8. References

Sharp, F., et al., 2014. The use and environmental impact of daylighting. *Journal of Cleaner Production*, *85*, 462-471. https://doi.org/10.1016/j.jclepro.2014.03.092

Littlefair, P. J., et al. 1994. The performance of innovative daylighting systems, Renewable Energy 5.5-8: 920-934. https://doi.org/10.1016/0960-1481(94)90113-9

Mayhoub, M. S. 2014. Innovative daylighting systems' challenges: A critical study. Energy and buildings 80: 394-405. https://doi.org/10.1016/j.enbuild.2014.04.019

Kim, J. T., & Kim, G., 2010. Overview and new developments in optical daylighting systems for building a healthy indoor environment. Building and environment, 45(2), 256-269. https://doi.org/10.1016/j.buildenv.2009.08.024

Garcia-Fernandez, B., & Omar, O., 2023. Integrated innovative solar lighting system for optimization of daylight utilization for public library in Alexandria, Egypt. Ain Shams Engineering Journal, 14(1), 101819. https://doi.org/10.1016/j.asej.2022.101819

Osama Omar, et al., 2018. Optimization of Daylight Utilization in Energy Saving, Application on the Library in Faculty of Architecture, Design and Built Environment, Beirut Arab University, Alexandria Engineering Journal, 57(4), 3921-3930, ISSN: 1110-0168. https://doi.org/10.1016/j.aej.2018.10.00

Nair, M. G., et al., 2014. Classification of indoor daylight enhancement systems. Lighting Research & Technology, 46(3), 245-267. https://doi.org/10.1177/1477153513483299

Xie B. et al., 2015. Design of a brightness-enhancement-film-adaptive freeform lens to enhance overall performance in direct-lit light-emitting diode backlighting, Applied optics, 54(17), 5542-5548. https://doi.org/10.1364/AO.54.005542

Wang Y.J: et al. 2015. High directional backlight using an integrated light guide plate, Optics Express 23.2 1567-1575. https://doi.org/10.1364/OE.23.001567

García-Fernández, B., et al. 2015. Light losses in hollow, prismatic light guides related to prism defects: a transmittance model. Chinese Optics Letters, 13(9), 092201. http://dx.doi.org/10.3788/COL201513.092201

Dupertuis, M. A et al. 1994. Generalization of complex Snell–Descartes and Fresnel laws. JOSA A, 11(3), 1159-1166. https://doi.org/10.1364/JOSAA.11.001159

De Greve, B. 2006. Reflections and refractions in ray tracing. Retrived Oct, 16, 2014.

Born, M. & Wolf. E. 2013. Principles of optics: electromagnetic theory of propagation, interference and diffraction of light. Elsevier. ISBN 0-08-026482. https://doi.org/10.1063/1.1325200

Energy saving: EU action to reduce energy consumption. https://www.europarl.europa.eu (Accessed: November 12, 2024)

TracePro® Opto-Mechanical Design Software. https://lambdares.com/tracepro (Accessed: November 12, 2024)